ELSEVIER

Journal of Crystal Growth 243 (2002) 108–116

JOURNAL OF CRYSTAL GROWTH

www.elsevier.com/locate/jcrysgro

Magnetic stabilization of the buoyant convection in the liquid-encapsulated Czochralski process

J.S. Walker[a,*], D. Henry[b], H. BenHadid[b]

[a] *Department of Mechanical and Industrial Engineering, University of Illinois, 1206 West Green Street, Urbana, IL 61801, USA*
[b] *Laboratoire de Mécanique des Fluides et d'Acoustique, UMR CNRS 5509, Ecole Centrale de Lyon/Université Claude Bernard-Lyon 1, ECL, BP 163, 69131 Ecully Cedex, France*

Received 10 October 2001; accepted 21 May 2002
Communicated by J.J. Derby

Abstract

This paper presents a linear stability analysis for the buoyant convection during the liquid-encapsulated Czochralski growth of compound semiconductor crystals with a steady, uniform, vertical magnetic field. Results are presented for two values of the Prandtl number, corresponding to indium-phosphide (InP) and gallium-arsenide (GaAs). Most of the results are for a melt depth equal to the crucible diameter, but some results are also presented for a smaller depth. For the cases considered here, the instability involves a transition from a steady axisymmetric flow to a steady nonaxisymmetric flow corresponding to the first Fourier mode in the azimuthal direction. For the weaker magnetic fields, the critical Rayleigh number is close to that for the Rayleigh–Bénard instability in a vertical cylinder. For the stronger magnetic fields, the critical Rayleigh number for GaAs is higher than that for InP because convective heat transfer in the GaAs base flow reduces the vertical temperature gradient.

PACS: 47.32; 47.65

Keywords: A1. Computer simulation; A1. Convection; A1. Magnetic fields; A2. Magnetic field assisted czochralski methods; B2. Semiconducting III–V materials

1. Introduction

Single crystals of compound III–V semiconductors, such as indium-phosphide (InP) and gallium-arsenide (GaAs), are often grown by the liquid-encapsulated Czochralski (LEC) process [1]. Application of a steady, uniform, vertical magnetic field during the LEC process often leads to crystals with fewer dislocations and less intense striations [2–6]. A magnetic field of sufficient strength eliminates hydrodynamic instabilities leading to steady or periodic nonaxisymmetric melt motions.

Several studies of hydrodynamic instabilities during the Czochralski growth of silicon crystals have emphasized: (1) the coupling of the buoyant convection with the melt motion driven by

*Corresponding author. Tel.: +1-217-333-7979; fax: +1-217-244-6534.
E-mail address: jswalker@uiuc.edu (J.S. Walker).

0022-0248/02/$ - see front matter
PII: S0022-0248(02)01487-2

rotation of the crystal about its vertical centerline [7–9] and (2) the coupling of the buoyant and thermocapillary convections [10]. There are many differences between Czochralski silicon growth and LEC compound semiconductor growth. First, for silicon there is a free surface between the periphery of the crystal–melt interface and the vertical crucible wall. The temperature-dependent surface tension of this free surface drives a thermocapillary convection, which plays a key role in the evaporation of SiO from the free surface of a silicon melt. For the LEC process, the annular region above the melt and between the outside radius of the crystal and the inside radius of the crucible is filled with a liquid boron-oxide encapsulant, which prevents evaporation of the volatile element (P or As). Since the viscosity of the liquid boron-oxide is enormous, viscous shear stresses in the encapsulant balance any variations of the interfacial tension of the encapsulant–melt interface with negligible velocity, so that there is no thermocapillary or solutocapillary convection in the LEC process. Second, in Czochralski silicon growth, the crystal is often rotated at 25–30 rpm in order to produce a radially uniform oxygen distribution in the crystal. In LEC compound semiconductor growth, the crystal is often rotated at a very small angular velocity, such as 4 rpm [5,6], to insure that the crystal remains cylindrical in spite of small deviations from axisymmetry in the temperature distribution. The melt motion driven by such small angular velocities is negligible compared to the buoyant convection. Koai et al. [11] treated the stability of the melt motion in the LEC process with the crucible rotating at 30 rpm, but in many LEC processes, the crucible either is not rotated [5,6] or is rotated at a few rpm to reduce the effects of slight deviations from axisymmetry in the heat flux from the heater which surrounds the crucible. Thus, we focus on the stability of the buoyant convection without thermocapillary convection and without rotation of the crystal or crucible.

Several papers [12–14] have presented numerical solutions for the Rayleigh–Bénard instability in a vertical cylinder with a hot bottom, a cold top and a thermally insulated vertical wall. For a height equal to the cylinder radius, the first instability involves a transition from zero velocity and pure thermal conduction to a steady, axisymmetric convection, while the second instability leads to a steady nonaxisymmetric flow. The effects of a steady, uniform, vertical magnetic field on the Rayleigh–Bénard problem have been studied experimentally by Dold and Benz [15] and theoretically by Touihri et al. [16]. The base-state temperature gradient is vertical for the Rayleigh–Bénard problem. The magnetic stabilization of the buoyant convection with an essentially horizontal base-state temperature gradient has been studied for a horizontal cylinder [17,18] and for a horizontal rectangular boat [19–22] with hot and cold ends, modelling the horizontal Bridgman process.

The temperature gradient in the LEC process has both axial and radial components, so LEC combines features of the Rayleigh–Bénard and horizontal Bridgman problems. Since the crystal lies above the melt and since single-crystal growth requires a significant axial temperature gradient in the melt at the growth interface, the melt is always unstably stratified. However, unlike the Rayleigh–Bénard problem, there is a melt motion for every value of the Rayleigh number, so that the first instability involves a transition from a steady, axisymmetric flow to a steady or periodic nonaxisymmetric flow, rather than a transition from zero velocity and pure thermal conduction.

We present results for two values of the Prandtl number, $Pr = \nu/\kappa$, where ν and κ are the kinematic viscosity and thermal diffusivity of the melt. These values are $Pr = 0.015$ for InP and $Pr = 0.068$ for GaAs [23]. Since the melt depth decreases during the LEC process and since the lowest critical value of the Rayleigh number, $Ra = g\beta(\Delta T)R^3/\kappa\nu$, occurs for the largest depth, we focus primarily on a melt depth equal to the inside diameter of the crucible, which might correspond to the initial maximum depth in an actual LEC process. Here $g = 9.81\,\mathrm{m/s^2}$, β is the volumetric expansion coefficient of the melt, (ΔT) is the difference between the maximum temperature in the melt and the solidification temperature, and R is the inside radius of the crucible. We present critical values of the Rayleigh number, Ra_{cr}, versus Hartmann

number, $Ha = BR(\sigma/\mu)^{1/2}$, for $0 \leqslant Ha \leqslant 50$, where B is the flux density of the steady, uniform, vertical magnetic field, while σ and μ are the electrical conductivity and dynamic viscosity of the melt. All boundaries are treated as electrical insulators, which neglects the small electrical conductivity of the crystal. The nonzero electrical conductivity of the crystal has no effect on the axisymmetric base flow or on any axisymmetric perturbation, but it does affect nonaxisymmetric perturbations because they involve nonzero electric potentials. Nonzero values of the electric potential at the crystal–melt interface drive electric currents through the crystal, and their circuits are completed through the melt. Since the electrical conductivity of the crystal is much less than σ, the electric currents in the crystal can be neglected for the small values of Ha considered here [24].

2. Problem formulation

In addition to the steady, uniform, vertical magnetic field produced by a solenoid around the crystal-growth furnace, there is an induced magnetic field produced by the electric current in the melt. The characteristic ratio of the induced magnetic field to the applied one is the magnetic Reynolds number, $R_m = \mu_p \sigma U R$, where μ_p is the magnetic permeability of the melt and U is a characteristic velocity for the buoyant convection. Since R_m is very small for all crystal-growth processes, the induced magnetic field can be neglected.

With the Boussinesq approximation, the dimensionless governing equations are:

$$\frac{\partial \mathbf{v}}{\partial t} + (\mathbf{v}\cdot\nabla)\mathbf{v} = -\nabla p + \frac{Ra}{Pr} T\hat{\mathbf{z}} + Ha^2(\mathbf{j}\times\hat{\mathbf{z}}) + \nabla^2\mathbf{v}, \tag{1a}$$

$$\frac{\partial T}{\partial t} + \mathbf{v}\cdot\nabla T = Pr^{-1}\nabla^2 T, \tag{1b}$$

$$\nabla\cdot\mathbf{v} = 0, \tag{1c}$$

$$\mathbf{j} = -\nabla\phi + \mathbf{v}\times\hat{\mathbf{z}}, \tag{1d}$$

$$\nabla\cdot\mathbf{j} = 0, \tag{1e}$$

where r, θ, z are cylindrical coordinates with the $z-$axis along the vertical centerline of the melt, with r and z normalized by R, and with the unit vectors $\hat{\mathbf{r}}, \hat{\theta}, \hat{\mathbf{z}}$ while t is time normalized by R^2/v. Here (1) $\mathbf{v}$ is the velocity normalized by v/R, (2) p is the deviation of the pressure from the hydrostatic pressure for the uniform reference density normalized by $\mu v/R^2$, (3) T is the deviation of the melt temperature from the solidification temperature normalized by (ΔT), (4) $\mathbf{j}$ is the electric current density normalized by $\sigma v B/R$ and (5) ϕ is the electric potential function or voltage normalized by vB.

The geometry used to model the LEC process is sketched in Fig. 1, where a is the dimensionless radius of the crystal and $2b$ is the dimensionless melt depth. The boundary conditions on velocity and electric current density are $\mathbf{v} = 0$ at $r = 1$ and at $z = \pm b$, $j_r = 0$ at $r = 1$ and $j_z = 0$ at $z = \pm b$. We assume that there is no heat flux from the bottom of the crucible and that there is a uniform heat flux from the vertical wall of the crucible. The melt loses heat by conduction and radiation through the semitransparent boron-oxide encapsulant. The magnitude of this heat loss varies greatly between processes. For example, Zhang et al. [25] and Prasad et al. [26] showed through modelling and experiments that convective heat transfer in the inert gas filling the furnace is

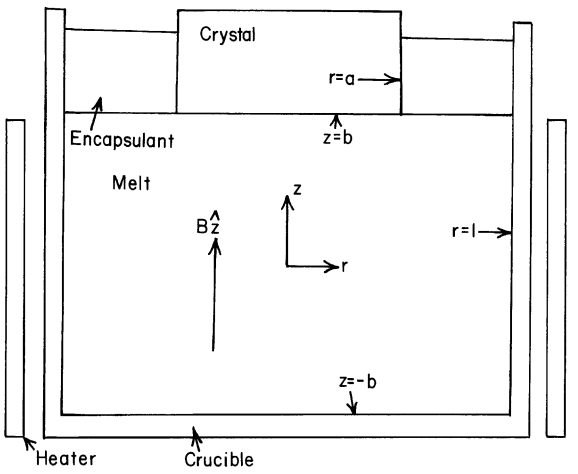

Fig. 1. Geometry with r and z normalized by the inside radius of the crucible and with the magnetic field $B\hat{z}$.

important for InP because the gas pressure is roughly 4.0 MPa, so that its density is large. On the other hand, GaAs is often grown with an inert gas pressure slightly above one atmosphere, so that convective heat transfer from the encapsulant is much smaller. A number of modellers have assumed that there is no heat flux across the encapsulant–melt interface, but Anselmo et al. [27] showed that this assumption leads to large errors for large values of *Ra*. Therefore, we assume that there is a uniform heat flux across the encapsulant–melt interface, so that the boundary conditions on T are:

$$\frac{\partial T}{\partial z} = 0 \quad \text{at } z = -b, \tag{2a}$$

$$\frac{\partial T}{\partial r} = q \quad \text{at } r = 1, \tag{2b}$$

$$T = 0 \quad \text{at } z = b \text{ for } 0 < r < a, \tag{2c}$$

$$\frac{\partial T}{\partial z} = -C \quad \text{at } z = b \text{ for } a < r < 1. \tag{2d}$$

We have made a rough estimate that $C = 0.2$ from previous models and experiments [25–27]. With our choice for (ΔT), the maximum value of T is one, so that we adjust the uniform heat flux q until this condition is satisfied for each steady, axisymmetric base-flow solution.

For v_r, v_z, p, T, j_θ, we introduce the form

$$v_r = v_{r0}(r,z) + \varepsilon\,\mathrm{Re}[\exp(\lambda t + \mathrm{i}m\theta)v_{r1}(r,z)], \tag{3a}$$

and for v_θ, ϕ, j_r, j_z, we introduce the form

$$v_\theta = \varepsilon\,\mathrm{Re}[\exp(\lambda t + \mathrm{i}m\theta)\mathrm{i}v_{\theta 1}(r,z)], \tag{3b}$$

where ε is an arbitrary small parameter, $\lambda = \lambda_\mathrm{r} + \mathrm{i}\lambda_\mathrm{i}$ is the possibly complex eigenvalue, m is the integer azimuthal wave number, the subscript 0 denotes the steady, axisymmetric base-flow variables and the subscript 1 denotes the possibly complex modal functions for the small perturbation. The i is included in Eq. (3b) so that if λ is real and if v_{z1} is real at one point, then all modal functions are real everywhere. These modal functions can be multiplied by $\exp(\mathrm{i}m\theta_0)$ which rotates a nonaxisymmetric perturbation in the azimuthal direction by an arbitrary angle θ_0. By setting $\theta_0 = 0$, we eliminate the arbitrary rotation for all nonaxisymmetric perturbations with no loss of generality.

For the steady, axisymmetric base flow, we introduce a streamfunction $\psi_0(r,z)$, where

$$v_{r0} = \frac{1}{r}\frac{\partial \psi_0}{\partial z}, \tag{4a}$$

$$v_{z0} = -\frac{1}{r}\frac{\partial \psi_0}{\partial r}. \tag{4b}$$

We cross-differentiate the r and z components of Eq. (1a) to eliminate p_0, so that we have a fourth-order azimuthal vorticity transport equation governing ψ_0 and Eq. (1b) governing T_0. The Taylor series expansions for T_0 and ψ_0 include only even powers of r, and that for ψ_0 starts with r^2. We used a Chebyshev spectral collocation method to solve for the base flow, where the Chebyshev polynomial representations had the correct Taylor-series behavior. Since the equations are nonlinear, we used a Newton–Raphson iterative method. As we increased *Ra* for fixed values of *Ha*, *Pr*, *a* and *b*, we obtained initial guesses for the coefficients in the representations by continuation from the converged solutions for smaller values of *Ra*, so that the Newton–Raphson method converged in a few iterations.

For the linearized perturbation equations neglecting $O(\varepsilon^2)$ terms and for $m \neq 0$, we eliminated $v_{\theta 1}$ with Eq. (1b), we eliminated $p_1$with the θ component of Eq. (1a), and we eliminated $j_{r1}, j_{\theta 1}, j_{z1}$ with Eq. (1d), leaving four linear, homogeneous equations governing $v_{r1}, v_{z1}, T_1, \phi_1$, with coefficients given by the base-flow variables and their derivatives. We reduced the four governing differential equations and the homogeneous boundary conditions to an eigenvalue matrix problem with a Chebyshev spectral collocation method. We found that the Chebyshev polynomial representations should have the correct Taylor series behavior in r, so that v_{r1} has the form

$$r^{(m-1)} \sum_L \sum_N A_{LN} T_{2L}(r) T_N(z/b) \tag{5a}$$

and v_{z1}, T_1, ϕ_1 have the form

$$r^m \sum_L \sum_N B_{LN} T_{2L}(r) T_N(z/b), \tag{5b}$$

where $T_k(x) = \cos[k \arccos(x)]$ are the Chebyshev

polynomials. We used a standard subroutine to find the real and complex eigenvalues for our matrix problem. For given values of Ha, Pr, a, and b, and for $m = 1$–8, we executed a search routine to find the value of Ra_{cr} for which the first eigenvalue has $\lambda_r = 0$. We also treated the $m = 0$ case in order to investigate if the first instability involves an axisymmetric perturbation, but this was not true for any case considered here.

In order to validate the numerical accuracy of our spectral collocation solutions for the base flow and for the eigenvalue problem, we changed the boundary conditions in order to duplicate two previous linear stability analyses for which numerical accuracy was thoroughly investigated. First, Prange et al. [28] presented a linear stability analysis for the steady, axisymmetric thermocapillary convection in a cylindrical liquid bridge between two circular surfaces at different temperatures and with a steady, uniform, axial magnetic field. The changes to our boundary conditions are that $T = \mp 0.5$ at $z = \pm b$ and that there is a thermally insulated free surface at $r = 1$, where the surface tension varies linearly with temperature. Without buoyant convection, the key parameter is a Reynolds number based on a characteristic velocity for the thermocapillary convection. For $b = 0.5$, $Pr = 0.02$ and $0 \leqslant Ha \leqslant 15$, Prange et al. [28] presented detailed information on their numerical accuracy. Our code with appropriate changes gives results for the critical value of the Reynolds number and for the characteristics of the perturbation variables, which are virtually identical to those presented by Prange et al. [28].

Second, Touihri et al. [16] presented a linear stability analysis for the Rayleigh–Bénard problem in a vertical cylinder with a steady, uniform, vertical magnetic field. The only changes to our boundary conditions are that $T = \mp 0.5$ at $z = \pm b$ and $\partial T/\partial r = 0$ at $r = 1$. Our code predicts the same values of Ra_{cr} for the first instability for every value of b, Ha and Pr which they considered, but this is not a severe test since the base state is zero velocity and pure thermal conduction. For $b = 0.5$, $Pr = 1.0$ and $0 < Ha < 12$, Touihri et al. [16] presented linear stability results for the secondary instability leading from a steady axisymmetric flow to a steady nonaxisymmetric flow with an $m = 2$ perturbation superimposed on the axisymmetric flow. Since this involves a transition from a steady axisymmetric flow to a nonaxisymmetric flow with a magnetic field, it represents a better test of our code and our code gives the same results.

3. Results

For all the results presented here, $a = 0.6$. The magnetic field strength required to eliminate buoyant instabilities throughout the LEC process is determined by the largest melt depth at the beginning of the process. Therefore we focus primarily on $b = 1$, where the melt depth equals the crucible diameter. The values of Ra_{cr} for $b = 1$, $Pr = 0.015$ or 0.068 and $0 \leqslant Ha \leqslant 50$ are presented in Fig. 2. For $0 \leqslant Ha \leqslant 15$, Ra_{cr} is the same for both

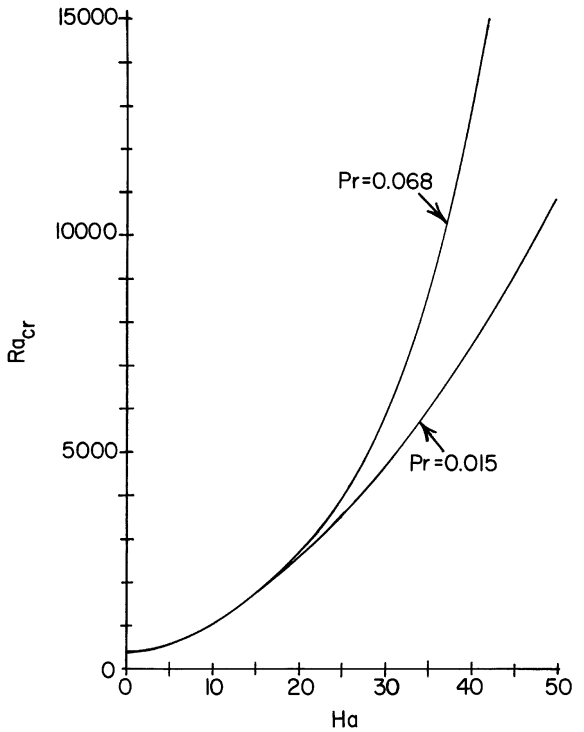

Fig. 2. Critical Rayleigh number versus Hartmann number for $b = 1$ and for two values of the Prandtl number.

values of Pr. For the Rayleigh–Bénard problem, Touihri et al. [16] presented a graph of Ra_{cr} versus Ha for $b = 1$ and $0 \leqslant Ha \leqslant 15$, and their curve coincides with our curve for this range of Ha. For example, they give $Ra_{cr} = 462.0$ [14] and 1345.9 [16] for $Ha = 0$ and 12.5, respectively, and these two points lie on our curve. This agreement with the Rayleigh–Bénard instability for $0 \leqslant Ha \leqslant 15$ apparently arises from compensating differences which are evident in the base-flow isotherms for LEC with $a = 0.6$ and $b = 1$. For both values of Pr and $0 \leqslant Ha \leqslant 15$, base-flow convective heat transfer is small at Ra_{cr}, so that the isotherms are nearly the same for these cases, and we present those for $Pr = 0.015$ and $Ha = 0$ in Fig. 3 as typical. At $z = 1$, T varies from 0.0 at $r = 0.6$ to 0.4 at $r = 1.0$, and at $z = -1$, T varies from 0.87 at $r = 0$ to 1.0 at $r = 1$, so that the average axial temperature gradient is smaller for LEC than for the Rayleigh–Bénard problem with the same (ΔT). On the other hand, the $T = 0.1$ isotherm intersects $r = 0$ at $z = 0.9$, rather than at $z = 0.8$, so that the axial temperature gradient along the centerline near the crystal–melt interface is twice that in the Rayleigh–Bénard problem, and the axial temperature gradient is even larger in the melt near $r = 0.5$ and $z = 1$. Thus the LEC melt is less unstable on average, but is more unstable over a significant volume of the melt below the crystal.

If we fix Ra and increase Ha, the magnitude of the steady, axisymmetric flow decreases. However, we are interested in the base flow at Ra_{cr} for each value of Ha. For the critical point as Ha is increased, the increase in the base-flow circulation due to the increase in Ra_{cr} is larger than the decrease due to increased magnetic damping, so that the base-flow circulation and the convective heat transfer both increase. As Ha is increased from 0 to 50, the maximum value of ψ_0 increases from 5.3 to 29.8 for $Pr = 0.015$ and from 1.55 to 31.2 for $Pr = 0.068$. Convective heat transfer makes the base-state isotherms more vertical and reduces the magnitude of the negative axial temperature gradient. For $Pr = 0.015$, convective heat transfer remains weak over this entire range, so that the base-state isotherms for $Ha = 50$ are still very similar to those in Fig. 3. Thus the curve for $Pr = 0.015$ in Fig. 2 can be considered the neutral stability curve for a nearly constant base-state temperature distribution. On the other hand, for $Pr = 0.068$, convective heat transfer begins to change the base-state isotherms for $Ha > 15$. The base-state isotherms for $Pr = 0.068$, $Ha = 50$ and $Ra_{cr} = 40995$ are presented in Fig. 4. There is now

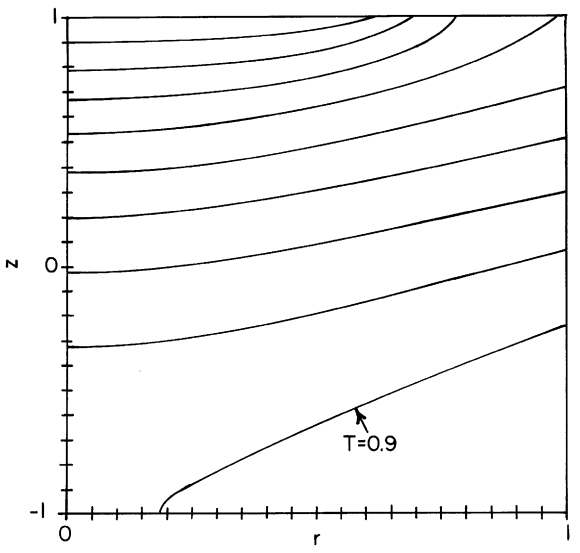

Fig. 3. Base-state isotherms at the critical point for $Pr = 0.015$, $b = 1$ and $Ha = 0$: $T = 0.1k$ for $k = 1$–9.

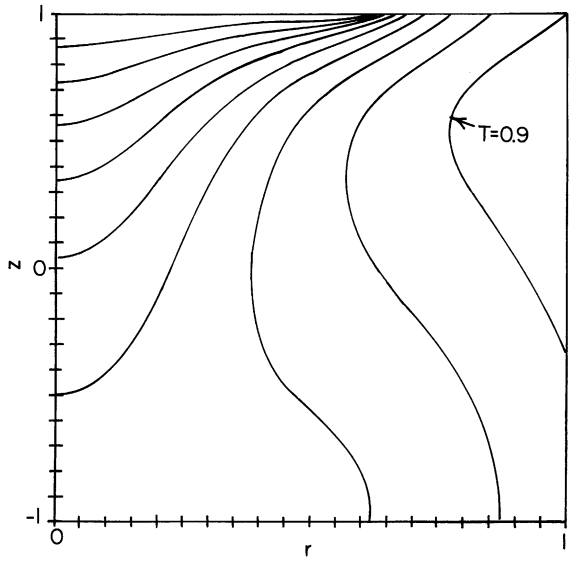

Fig. 4. Base-state isotherms at the critical point for $Pr = 0.068$, $b = 1$, $Ha = 50$: $T = 0.1k$ for $k = 1$–9.

a region of stably stratified melt, whose boundary is roughly defined by the vertical tangent points on the $T = 0.7$–0.9 isotherms. The axial temperature gradient at $r = 0$ in Fig. 4 is smaller for the entire depth than that in Fig. 3. There is a small region below the periphery of the crystal–melt interface where the axial temperature gradient has been increased by convective heat transfer. With much smaller and even positive axial temperature gradients over most of the melt, Ra must be increased to much larger values to reach the critical point, as indicated by the curve for $Pr = 0.068$ in Fig. 2. While Ra_{cr} is the same for $Pr = 0.015$ and 0.068 for $Ha < 15$, for $Ha = 50$, Ra_{cr} for $Pr = 0.068$ is nearly four times that for $Pr = 0.015$. Since convective heat transfer has very little effect on the base-state temperature distribution for $Pr = 0.015$ and $Ha = 50$ or for $Pr = 0.068$ and $Ha = 15$, we conclude: (1) that the entire neutral stability curve for $Pr = 0.015$ in Fig. 2 applies for $Pr < 0.015$, (2) that the common part of the curve for $Ha < 15$ applies for $Pr < 0.068$, and (3) that the Ra_{cr} at $Ha = 0$ applies to some higher, but undetermined value of Pr.

For all the cases in Fig. 2, $m = 1$ and $\lambda = 0$ for the critical perturbation, so that the instability leads from a steady, axisymmetric flow to a steady, nonaxisymmetric flow with an $m = 1$ perturbation superimposed on the base flow. Since the perturbation modal functions are real, the perturbations to v_r, v_z, T, p, j_θ have the form $v_{r1}(r,z)\cos\theta$, and the perturbations to v_θ, j_r, j_z, ϕ have the form $-v_{\theta 1}(r,z)\sin\theta$. After transition, the flow has one vertical plane of symmetry at $\theta = 0$ and $\theta = \pi$, recalling that we eliminated the arbitrary rotation by setting $\theta_0 = 0$. In addition, the small perturbation variables in the linear stability analysis are all either odd or even functions of $(\theta \pm \pi/2)$, although this characteristic would be eliminated by nonlinear effects as Ra is increased from Ra_{cr}.

Thus fluid rises for $|\theta| < \pi/2$, crosses the plane at $\theta = \pm\pi/2$ near $z = 1$ with $v_{\theta 1} < 0$, descends for $|\theta| > \pi/2$, and recrosses the plane at $\theta = \pm\pi/2$ near $z = -1$ with $v_{\theta 1} > 0$. For the Rayleigh–Bénard problem and for all values of Ha, $v_{\theta 1}$ for the first instability is an odd function of z [14,16]. For the LEC process with $Ha = 0$, the perturbation is fairly close to that for the Rayleigh–Bénard problem. For example, for $b = 1$, $Pr = 0.068$ and $Ha = 0$, $-0.74 \leqslant v_{\theta 1} \leqslant 0.61$ and the $v_{\theta 1} = 0$ contour runs from $z = -0.2$ at $r = 0$ to $z = 0.3$ at $r = 1$, so it is not too far from $z = 0$. Thus for $Ha = 0$ the critical $m = 1$ perturbation is close to a horizontal vortex with its axis in the $\theta = \pm\pi/2$ plane. We have normalized the perturbation variables with $v_{z1} = r$ at $r = 0.707$ and $z = 0$.

As Ha is increased, $v_{\theta 1}$ deviates much further from an odd function of z. The contours of $v_{\theta 1}$ for $b = 1$, $Pr = 0.015$, $Ha = 40$ and $Ra_{cr} = 7302.5$ are presented in Fig. 5. The flow from $|\theta| < \pi/2$ to $|\theta| > \pi/2$ is concentrated near $r = 0$ for $z > -0.5$ and the return flow is concentrated near $r = 1$ for $z < 0.4$. Vorticity which is perpendicular to a magnetic field is much more strongly damped than vorticity which is parallel to the field. As Ha is increased from 0 to 50, the horizontal component of the perturbation vorticity decreases and the vertical component increases. Thus the fluid for $|\theta| < \pi/2$ rises and moves radially inward, while the fluid for $|\theta| > \pi/2$ descends and moves radially outward. The Hartmann layers with $O(Ha^{-1})$ thickness at $z = \pm 1$ are evident in Fig. 5 and are equally evident in the contours of v_{r0} and v_{r1}.

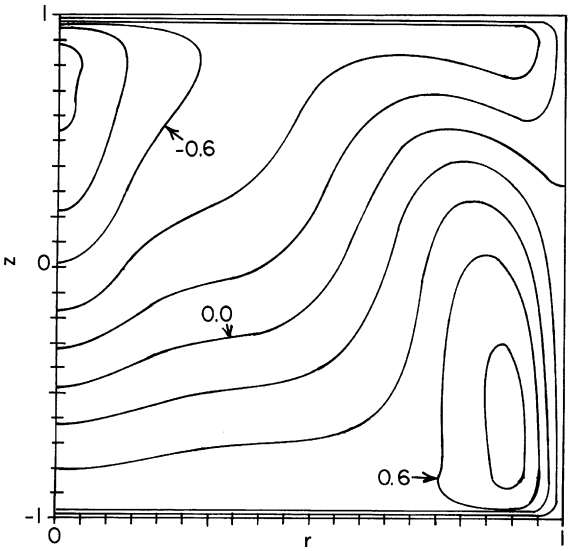

Fig. 5. Contours of $v_{\theta 1}$ for $b = 1$, $Pr = 0.015$, $Ha = 40$ and $Ra_{cr} = 7302.5$: $v_{\theta 1} = 0.2k$ for $k = -5$ to 4.

For $b = 0.67$ and $Ha = 0$, Touihri et al. [14] give $Ra_{cr} = 1435$ for all values of Pr, while $\lambda = 0$ and $m = 1$ for the critical perturbation in the Rayleigh–Bénard problem. For the LEC process with $b = 0.67$, $Ha = 0$ and $Pr = 0.068$, we found that $Ra_{cr} = 2206$, while again $\lambda = 0$ and $m = 1$ for the critical mode. Even for $Ha = 0$, there is significant convective heat transfer in the LEC base flow and there is stably stratified region near $r = 1$. Thus for $Ha = 0$, $b = 0.67$ and $Pr = 0.068$, the LEC problem has a higher value of Ra_{cr} than the Rayleigh–Bénard problem. As Ha is increased to 20 for the LEC problem with $b = 0.67$ and $Pr = 0.068$, convective heat transfer in the base flow at the critical point increases dramatically and Ra_{cr} increases to 20 814. The maximum and minimum values of v_{r0} for the critical state with $Pr = 0.068$, $b = 0.67$ and $Ha = 20$ are more than twice as large as those for the critical state with $Pr = 0.068$, $b = 1$ and $Ha = 50$. For $b = 0.67$, $Ha = 20$ and $Pr = 0.068$, more than half of the melt is stably stratified, and there is only a small region near the periphery of the crystal–melt interface where the negative axial temperature gradient is larger than that for the Rayleigh–Bénard problem. The important points are: (1) that Ra_{cr} is much larger for $b = 0.67$ than it is for $b = 1.0$, so that the melt with the largest depth requires the strongest magnetic field for stability and (2) that the increase in Ra_{cr} with a given decrease in b is larger than that for the Rayleigh–Bénard problem because convective heat transfer in the base flow at the critical point increases as b is decreased, thus reducing the negative axial temperature gradient.

4. Concluding remarks

The results presented here show that a steady, uniform, vertical magnetic field can dramatically increase the critical value of the Rayleigh number for the first instability in the steady, axisymmetric buoyant convection during the LEC growth of compound semiconductor crystals. However, our calculations are still quite far from reality. For the magnetically stabilized process for InP developed by Bliss and colleagues [5,6,25,26], $Ra = 5.24 \times 10^6$ and $Ha = 687$. Much more research will be needed in order to develop accurate predictions of Ra_{cr} and of the characteristics of the first instability for such large values of Ha.

For the thermocapillary convection in a cylindrical liquid bridge, Prange et al. [28] could only obtain accurate numerical results for $Ha \leqslant 15$ due to the dramatic growth of spatial resolution requirements with increasing values of Ha. For the buoyant convection in the LEC process, we were able to obtain accurate results for $Ha \leqslant 50$ with roughly the same spatial resolution as that of Prange et al. [28]. The resolution equivalence is approximate because they use spectral representations in the radial direction and finite-difference representations in the axial direction, while we use spectral representations with Gauss-Lobatto collocation points in both directions. The future modelling of the magnetic stabilization of buoyant or thermocapillary convections in crystal-growth processes with larger values of Ha should be guided by a thorough undertanding of magnetohydrodynamics [29].

The value of Ra_{cr} depends on the base-flow temperature distribution, which depends on the thermal boundary conditions. Here, we have only considered one set of thermal boundary conditions corresponding to one process [25–27]. Realistic thermal boundary conditions for other LEC processes might be quite different, leading to very different results for Ra_{cr}. For example, for some processes, the initial melt depth is small and there is significant heat input at the crucible bottom from a heater below the crucible. Such bottom heat input would bring the problem closer to the Rayleigh–Bénard problem.

Gelfgat et al. [30] recently presented a linear stability analysis for the buoyant convection in a cylinder with isothermal top and bottom at the same temperature, with a parabolic temperature variation along the vertical wall of the cylinder, with a vertical magnetic field and with $Pr = 0.015$. For $b = 1$, they found that m for the critical instability changed from 2 to 0 to 6 to 7 as Ha was increased from 0 to 40, while $m = 1$ throughout this range for our thermal boundary conditions. In addition they found that $Ra_{cr} = 72450$ for $Ha = 40$, which is an order of magnitude larger than the

Ra_{cr} in Fig. 2. This illustrates the strong dependence of the instability on the thermal boundary conditions.

The present assumption of axisymmetric thermal boundary conditions may not be realistic for some actual processes since many heaters have a gap leading to less heat input at one azimuthal location. Even a small deviation from axisymmetry in the temperature distribution may lead to a large deviation from axisymmetry in the melt motion with a vertical magnetic field [31,32]. With a heat input which varies as $\cos\theta$, the steady base flow would be three dimensional and there would probably not be an instability corresponding to the first instability for an axisymmetric base flow. The first instability might involve the transition to periodic melt motions. Clearly more research is needed to explore the instability of steady, three-dimensional base flows with nonaxisymmetric thermal boundary conditions.

Acknowledgements

This research was supported by the US National Science Foundation under Grant CTS-0129028 and by the US National Aeronautics and Space Administration under Grants NAG8-1453 and NAG8-1705. The calculations were performed on a workstation donated by the International Business Machines Corporation.

References

[1] D.T.J. Hurle, B. Cockayne, Handbook of Crystal Growth, Vol. 2, Elsevier Science B.V, Amsterdam, 1994, p. 99.
[2] T. Kimura, T. Katsumata, M. Nakajima, T. Fukuda, J. Crystal Growth 79 (1986) 264.
[3] H. Miyairi, T. Inada, M. Eguchi, T. Fukuda, J. Crystal Growth 79 (1986) 291.
[4] D.J. Carlson, A.F. Witt, J. Crystal Growth 116 (1992) 461.
[5] D.F. Bliss, R.M. Hilton, J.A. Adamski, J. Crystal Growth 128 (1993) 451.
[6] D.F. Bliss, R.M. Hilton, S. Bachowski, J.A. Adamski, J. Electron. Mater. 20 (1991) 967.
[7] T. Munakata, I. Tanasawa, J. Crystal Growth 106 (1990) 566.
[8] K. Kakimoto, M. Watanabe, M. Eguchi, T. Hibiya, J. Crystal Growth 126 (1993) 435.
[9] A. Seidl, G. McCord, G. Müller, H.J. Leister, J. Crystal Growth 137 (1994) 326.
[10] K.W. Yi, K. Kakimoto, M. Eguchi, M. Watanabe, T. Shyo, T. Hibiya, J. Crystal Growth 144 (1994) 20.
[11] K. Koai, A. Seidl, H.J. Leister, G. Müller, A. Köhler, J. Crystal Growth 137 (1994) 41.
[12] G. Neumann, J. Fluid Mech. 214 (1990) 559.
[13] M. Wanschura, H.C. Kuhlmann, H.J. Rath, J. Fluid Mech. 326 (1996) 399.
[14] R. Touihri, H. Ben Hadid, D. Henry, Phys. Fluids 11 (1999) 2078.
[15] P. Dold, K.W. Benz, Cryst. Res. Technol. 30 (1995) 1135.
[16] R. Touihri, H. Ben Hadid, D. Henry, Phys. Fluids 11 (1999) 2089.
[17] H. Ben Hadid, D. Henry, R. Touihri, J. Crystal Growth 180 (1997) 433.
[18] L. Davoust, M.D. Cowley, R. Moreau, R. Bolcato, J. Fluid Mech. 400 (1999) 59.
[19] D.T.J. Hurle, E. Jakeman, C.P. Johnson, J. Fluid Mech. 64 (1974) 565.
[20] H. Ben Hadid, D. Henry, S. Kaddeche, J. Fluid Mech. 333 (1997) 23.
[21] H. Ben Hadid, D. Henry, J. Fluid Mech. 333 (1997) 57.
[22] A. Juel, T. Mullin, H. Ben Hadid, D. Henry, J. Fluid Mech. 378 (1999) 97.
[23] A.S. Jordan, J. Crystal Growth 71 (1985) 551.
[24] L.N. Hjellming, J.S. Walker, J. Fluid Mech. 164 (1986) 237.
[25] H. Zhang, V. Prasad, D.F. Bliss, J. Crystal Growth 169 (1996) 250.
[26] V. Prasad, D.F. Bliss, J.A. Adamski, J. Crystal Growth 142 (1994) 21.
[27] A. Anselmo, V. Prasad, J. Koziol, K.P. Gupta, J. Crystal Growth 134 (1993) 116.
[28] M. Prange, M. Wanschura, H.C. Kuhlmann, H.J. Rath, J. Fluid Mech. 394 (1999) 281.
[29] R. Moreau, Magnetohydrodynamics, Kluwer Academic Publishers, Dordrecht, 1990.
[30] A.Yu. Gelfgat, P.Z. Bar-Yoseph, A. Solan, J. Crystal Growth 230 (2001) 63.
[31] N. Ma, J.S. Walker, Phys. Fluids 7 (1995) 2061.
[32] N. Ma, J.S. Walker, J. Fluids Eng. 118 (1996) 155.